Pseudomonas aeruginosa AlgF is a protein-protein interaction mediator required for acetylation of the alginate exopolysaccharide

Kristin E. Low[1†#], Andreea A. Gheorghita[1,2†,#], Stephanie D. Tammam[1†], Gregory B. Whitfield[1,2†#], Yancheng E. Li[2#], Laura M. Riley[1#], Joel T. Weadge[1#], Shane J. Caldwell[1#], P. Andrew Chong[1], Marthe T. C. Walvoort[3#], Elena N. Kitova[4], John S. Klassen[4], Jeroen D. C. Codée[3], P. Lynne Howell[1,2]*

[1] *Program in Molecular Medicine, The Hospital for Sick Children, Toronto, Ontario, Canada;* [2] *Department of Biochemistry, University of Toronto, Toronto, Ontario, Canada;* [3] *Leiden Institute of Chemistry, Leiden University, Leiden, The Netherlands;* [4] *Alberta Glycomics Centre and Department of Chemistry, University of Alberta, Edmonton, Alberta, Canada*

† These authors contributed equally to this work.

Present addresses: K.E.L: Lethbridge Research and Development Centre, Agriculture and Agri-Food Canada, Lethbridge, Alberta, Canada; A.A.G.: Research Institute of Molecular Pathology, Vienna Biocenter, 1030 Vienna, Austria; G.B.W.: Département de Microbiologie, Infectiologie, et Immunologie, Université de Montréal, Montréal, Québec, Canada; Y.E.L.: Division of Chemistry and Chemical Engineering, California Institute of Technology, Pasadena, California, USA; L.M.R.: Ontario Genomics, Toronto, Ontario, Canada; J.T.W.: Department of Biology, Wilfrid Laurier University, Waterloo, Ontario, Canada; S.J.C: Amgen British Columbia, Burnaby, British Columbia, Canada; M.T.C.W: Stratingh Institute for Chemistry, University of Groningen, Groningen, The Netherlands.

* To whom correspondence should be addressed: P. Lynne Howell, howell@sickkids.ca

ABSTRACT

Enzymatic modifications of bacterial exopolysaccharides enhance immune evasion and persistence during infection. In the Gram-negative opportunistic pathogen *Pseudomonas aeruginosa*, acetylation of alginate reduces opsonic killing by phagocytes and improves reactive oxygen species scavenging. Although it is well-known that alginate acetylation in *P. aeruginosa* requires AlgI, AlgJ, AlgF, and AlgX, how these proteins coordinate polymer modification at a molecular level remains unclear. Here, we describe the structural characterization of AlgF and its protein interaction network. We characterize direct interactions between AlgF and both AlgJ and AlgX *in vitro*, and demonstrate an association between AlgF and AlgX, as well as AlgJ and AlgI, in *P. aeruginosa*. We determine that AlgF does not exhibit acetylesterase activity and is unable to bind to polymannuronate *in vitro.* Therefore, we propose that AlgF functions to mediate protein-protein interactions between alginate acetylation enzymes, forming the periplasmic AlgJFXK (AlgJ-AlgF-AlgX-AlgK) acetylation and export complex required for robust biofilm formation.

INTRODUCTION

Biofilms are communities of bacterial cells surrounded and protected by a self-produced matrix containing lipids, exopolysaccharides, extracellular DNA, and proteins, and more complex structures such as membrane vesicles, bacteriophage, and amyloid fibres (1–3). The biofilm matrix promotes adhesion and cohesion of bacterial cells, and permits bacteria to adapt and thrive as a multicellular community despite environmental stresses (2, 4, 5). Bacterial biofilms can form in a variety of environments, including niches relevant to human health. They can grow on solid surfaces (e.g., medical devices), at an air-liquid interface (e.g., dental biofilms), or within semi-solid media (e.g., sputum in the lungs of individuals with cystic fibrosis (CF) during chronic infection with *Pseudomonas aeruginosa*) (2).

Modification of exopolysaccharides within the biofilm confers protection to pathogenic bacteria during infection (6). Deacetylation of poly-*N*-acetyl-glucosamine (PNAG) is required for biofilm formation in *Streptococcus epidermidis*, *Streptococcus aureus*, *Escherichia coli*, and *Yersinia pestis*, and provides

resistance to neutrophil phagocytosis and enhances persistence in a mouse model of infection for *S. epidermidis* and *S. aureus* (6–10). Acetylation is another common modification. For example, acetylation of *Vibrio* polysaccharide is required for biofilm formation in *Vibrio cholerae* (11) and acetylation of cellulose is required for surface colonization in *Pseudomonas fluorescens* (12). Acetylation of alginate in *P. aeruginosa* is not only involved in forming the mature biofilm structure (13, 14), but also reduces opsonic killing by phagocytes, reduces susceptibility to enzymatic degradation, and aides in scavenging reactive oxygen species (6, 15–17).

In *P. aeruginosa*, alginate acetylation is known to require four proteins, AlgI, AlgJ, AlgF, and AlgX (18–22). Belonging to the membrane-bound *O*-acetyltransferase (MBOAT) family of proteins (18, 21), AlgI is hypothesized to receive an acetyl group from an unknown donor in the cytoplasm and transfer it to AlgJ in the periplasm (23). Although AlgJ exhibits acetylesterase activity *in vitro*, AlgJ is unable to bind or acetylate poly-mannuronate oligomers *in vitro*, suggesting that it is an intermediary in alginate acetylation (20). AlgX is a periplasmic acetyltransferase that can remove an acetyl group from an artificial donor and transfer it onto mannuronate polymer *in vitro.* In addition, chromosomal mutation of AlgX residues required for its acetyltransferase activity led to production of non-acetylated alginate (19, 20). Thus, it has been hypothesized that a relay takes place to transfer an acetyl group from the cytoplasm to the polysaccharide chain, via AlgI, AlgJ and finally AlgX (18–20). AlgF is also localized to the periplasm and is required for alginate acetylation *in vivo*, but little is known about its structure or function to date (18, 22).

Here, we describe the structure of AlgF determined by CS-Rosetta from chemical shifts data (24) and supported by interproton nuclear Overhauser effect (NOE) analysis. We demonstrate protein-protein interactions *in vitro* between AlgF and AlgJ, as well as AlgF and AlgX, by isothermal titration calorimetry (ITC), and an interaction between AlgF and AlgX identified by co-immunoprecipitation (co-IP) in *P. aeruginosa*. Based on these results, we propose that AlgF functions to mediate interactions

between AlgJ and AlgX that are critical for the acetyl relay mechanism required for alginate acetylation, insights that allow us to propose the most detailed model yet of how alginate is modified prior to export.

RESULTS

AlgF consists of two β-sandwich domains joined by a short linker region.

AlgF is annotated as a periplasmic *O*-acetyltransferase in the *Pseudomonas* Genome Database for several species, including *P. aeruginosa* and *Pseudomonas putida* (25). This annotation is probably due to its demonstrated role in alginate acetylation (18), but sequence alignments with the previously characterized *O*-acetyltransferases AlgJ (20) and AlgX (19, 20) reveal that AlgF lacks similarity to these and other known acetyltransferases. To gain insight into the role of AlgF in alginate acetylation we first determined its structure. Despite exhaustive attempts, the protein proved to be recalcitrant to crystallization, and therefore CS-Rosetta models (26) were generated and validated using NMR spectroscopic techniques.

Uniformly ^{1}H,^{15}N, and ^{13}C labeled *P. aeruginosa* AlgF lacking its signal sequence, $AlgF_{Pa}^{30-216}$, was expressed and purified. Backbone, triple, and side-chain resonances were assigned by NMR (see Methods) and NOE distance restraints were collected for structural modelling (26–35). $AlgF_{Pa}$ chemical shifts were assigned to 94.6% completeness. Analysis of the chemical shift data using the chemical shift index (CSI) as calculated by NMRView (28, 30) (Figure S1) indicated that the N- and C-termini were not involved in any stable secondary structural elements as the CSI values were close to zero, as expected for regions with random coil characteristics. Sequence analysis revealed that the protein contains repeating homologous segments, suggesting the presence of a pair of tandem domains joined by a short interdomain region (Figure 1A). The termini and the interdomain region (as well as many loop/turn regions) did not show any long-range NOE assignments (assignments more than four amino acid residues away in sequence) indicating that these regions are only in close contact with their sequential neighbours (Figure S1). Analysis of the folded regions suggested that the structure was all β-strand as reflected by positive CSI scores and a lack of NOE patterns typically found in helical structures (*i.e.* backbone interproton

NOEs seen between residues 3 or 4 amino acids apart, i-i+3 and i-i+4 in Figure S1). There is good agreement with the secondary structure observed in the early atomic models calculated using NOE-derived distance restraints (Figure S1, bottom row) and chemical shift data analysis. Despite the quality of the data there were an unacceptable number of clashes and NOE distance restraint violations in ensembles calculated using NOE derived restraints in CYANA (27) (Table 1). This is probably the consequence of the 32% sequence identity between the N- and C-terminal domains (Figure 1A), which results in a high degree of overlap in many chemical shifts resonances. Given the ~95% completeness of the chemical shift assignments, these data were therefore used in conjunction with the CS-Rosetta server to calculate structural models (26). As is typical for multidomain proteins, when the chemical shift data for the full-length protein was submitted to CS-Rosetta the algorithm failed to converge on a single structure. However, separating the shift data for the two domains provided well-converged structures that matched the NMR restraint-derived structures (Figure 1B and C) with backbone root-mean-square deviations (RMSD) of 1.6 Å and 1.7 Å between the lowest energy CS-Rosetta and NMR-derived N-terminal and C-terminal domain models, respectively. All calculations using NOE-derived distance restraints gave ensembles consisting of two tandem domains (Figure 1). Four amino acids connect the two domains that we could not resolve structurally. Despite extensive searching, no unambiguous interdomain NOE assignments could be found. These results are either because no interdomain NOEs exist, or the structural and sequence similarity between the domains resulted in overlapping chemical shift assignments obscuring the inter-domain NOE assignments.

Both the N- and C-terminal domains of $AlgF_{Pa}$ form an 8-stranded β-sandwich with backbone ensemble RMSDs for the CS-Rosetta determined models of 1.4 Å and 1.6 Å, respectively (Figures 2A, S2 and Table 1). The $AlgF_{Pa}$ β-sandwich has two distinct sides; one side is flatter with longer strands (β1, β4, β7, and β8), while the other side has a slight curve with shorter strands and longer loops (β2, β3, β5, and β6) (Figure S2). This asymmetric β-sandwich with one flat face and one curved face was found in both the

CS-Rosetta and NOE derived models (Figure 1). The N- and C-terminal domains are structurally similar to each other and superpose with an average ensemble backbone RMSD of 2.1 Å (Figure 2A). Superimposition of the N- and C-terminal domains with the AlphaFold (36) model of $AlgF_{Pa}$ which predicts the structure with high confidence (Figure S3), reveals a backbone RMSD of 1.5 and 1.6 Å, respectively (Figure 2B). Overall, comparison to the AlphaFold model suggests that the N- and C-terminal domains interact to form a compact structure.

To gain insight into the function of $AlgF_{Pa}$, the surface characteristics of each domain were further analyzed with respect to charge and sequence conservation. The theoretical pI values were calculated to be 4.60 and 9.61 for the N- and C- terminal domains, respectively, and these differences are reflected in the calculated coulombic surface potential maps (Figure 2C). The N-terminal domain of $AlgF_{Pa}$ has patches of negatively and positively charged residues, while the C-terminal domain is mostly positively charged. Using the ConSurf server (37), we identified highly conserved surface patches on both N- and C-terminal domains (Figure 2D and 2E). When conservation was analyzed in the context of the compact AlphaFold2 $AlgF_{Pa}$ structure, highly conserved patches on both domains become buried, further suggesting that the two domains interact (Figure S4). Specifically, the highly conserved residues Arg46, Ala50, Ser72, Ser73, and Val105 on the N-terminal domain and Asn132, Leu133, Val209, and Arg211 on the C-terminal domain are buried in the AlphaFold $AlgF_{Pa}$ model (Figure S4A). Of these highly conserved residues, Arg46 on the N-terminal domain and Arg211 and Asn132 on the C-terminal domain are involved in electrostatic interactions (Figure S4B). The most electropositive/electronegative regions of AlgF are not involved in mediating interactions between the two domains. The highly conserved residues Val105 on the N-terminal domain and Val209 and Leu133 on the C-terminal domain are involved in hydrophobic interactions (Figure S4C). Less conserved residues, Tyr48 and Val115 on the N-terminal domain and Tyr196 and Val207 on the C-terminal domain, are also involved in hydrophobic interactions between the two domains (Figure S4C). Analysis of the $AlgF_{Pa}$ AlphaFold model by the Proteins, Interfaces, Surfaces, and Assemblies (PISA) server (38) also predicts that the N- and C-terminal domains

interact, with an interaction interface buried surface of 752.4 Å^2. PISA indicates that the following residues become buried or are solvent inaccessible in the interaction interface: Arg46, Tyr48, Ala50, Ser72, Ser73, Val105 and Val115 on the N-terminal domain are buried, while Leu133, Tyr196, Val207, Val209, and Arg211 on the C-terminal domain are buried (Figure S4D). These data support a compact AlgF structure where the N- and C-terminal domains interact.

Structurally similar proteins are involved in protein-protein and/or protein-ligand interactions.

The AlgF$_{Pa}$ CS-Rosetta and AlphaFold2 models were submitted individually to the DALI server (39, 40) to identify structurally similar proteins. Based on the nature of ligands bound, we identified four different classes that represent most of the hits identified: 1, protein-binding (e.g. PepT2 solute carrier family 15 extracellular domains, BcpA); 2, cholesterol-binding (e.g. pneumolysin); 3, carbohydrate-binding (e.g. rhamnogalacturonase); and 4, hormone/vitamin-binding (e.g. transthyretin) (Figure 3). Although all four classes contain structurally similar β-sandwich domains, each class is capable of binding chemically distinct ligands.

Class 1 proteins have the most structural homology to AlgF$_{Pa}$. Within class 1, solute carrier family 15 proteins (PepT1 and PepT2 (41)) are involved in oligopeptide transport across mammalian cell membranes and the extracellular domains of these proteins bind trypsin and recruit it to the site of dietary peptide uptake. PepT1 and PepT2 extracellular regions consist of two tandem β-sandwich domains joined by a short linker, and most closely resemble the β-sandwich domain structure of AlgF$_{Pa}$ (Figure S5A). However, only PepT2's domains appear to interact to form a compact particle, similar to AlgF$_{Pa}$ (Figure S5A). Despite the similar structures, PepT1 and PepT2 share 19% and 14% amino acid sequence identity, respectively, to the AlgF N-terminal domain. Sequence comparisons to the AlgF$_{Pa}$ C-terminal domain are similar; 14% and 16% for PepT1 and PepT2, respectively. The bacterial pilin adhesion protein BcpA is critical for maintaining cell-cell contacts through intramolecular amide bonds, resulting in pili fibre

formation on the cell surface (42). While BcpA has three tandem β-sandwich domains which are structurally similar to the N-terminal and C-terminal domains of $AlgF_{Pa}$, the amino acid sequence identity between any two of the aligned domains is less than 6%. Class 2 consists of cholesterol-binding proteins including pneumolysin, a toxin found in pathogenic *Streptococcus pneumoniae* that forms a pore in eukaryotic membranes (43). Only the cholesterol-binding domain of the toxin forms a β-sandwich that is structurally similar to the N-terminal and C-terminal domains of $AlgF_{Pa}$. Domain II of rhamnogalacturonase in class 3 is suggested to be involved in oligosaccharide binding and resembles a single domain of AlgF (22, 23). The class 4 protein transthyretin is named for its role in transporting thyroxine and retinol in serum (44). While transthyretin consists of β-sandwich structures, the domains are oriented differently compared to $AlgF_{Pa}$ (Figure S5B) (44). Most of the remaining unclassified hits (*i.e.* not belonging to classes 1-4) also have a role in binding small molecules and have little similarity to the structure of AlgF. In the case of multi-domain proteins identified by the DALI search, the AlgF-like β-sandwich domain functions to bind small molecules, while the rest of the respective protein carries out the biological function. Since AlgF lacks any ancillary domains, we hypothesize that it most likely functions solely to bind either a small molecule or protein ligand.

In vitro binding analyses reveal direct interactions between AlgF, AlgJ, and AlgX.

Since class 1 proteins with a β-sandwich structure are involved in binding proteins and AlgF has been proposed to interact with the acetylation machinery (45), we next investigated whether AlgF is involved in protein-protein interactions. Binary interactions between *P. putida* homolog constructs $AlgF_{Pp}^{30\text{-}215}$, $AlgJ_{Pp}^{75\text{-}370}$, and $AlgX_{Pp}$ were probed *in vitro* using isothermal titration calorimetry (ITC). These proteins could be obtained in higher yields and were more stable than their *P. aeruginosa* counterparts thus enabling the ITC experiments (Figure 4). We found that $AlgJ_{Pp}$ and $AlgX_{Pp}$ bind to $AlgF_{Pp}$ with K_d values of 86 ± 12 μM and 178 ± 5 μM, respectively. Titration of $AlgX_{Pp}$ into $AlgJ_{Pp}$ demonstrated a decreasing heat of enthalpy as the titration proceeded, however the data could not be reliably fit as the heats of

emission were small and the titration did not reach saturation. The data suggest a weak interaction with a dissociation constant in the mM range.

AlgF is not an acetyltransferase and does not bind alginate.

In Δ*algF* strains of *P. aeruginosa*, previous studies found that alginate exopolysaccharide is produced but not acetylated (18). The fold of AlgF did not suggest a particular enzymatic role and the 3D structure alone was not sufficient to provide insight into the function of AlgF. Unlike AlgJ and AlgX, AlgF shared no structural similarities with acetyltransferase enzymes. As AlgF is required for alginate acetylation, we investigated if this requirement was the result of a previously uncharacterized enzymatic activity.

An assay was carried out to determine whether $AlgF_{Pp}$ had acetylesterase activity, the first step in the acetyltransferase reaction. Removal of an acetate group from the pseudosubstrate 3-carboxyumbelliferyl acetate results in release of a fluorescent product, and reaction progress can be monitored through fluorescence spectroscopy. The acetylesterase activity of *P. aeruginosa* $AlgF_{Pp}$, $AlgX_{Pp}$, and $AlgJ_{Pp}$ was measured independently, in combination, and in the presence of an acetyl group acceptor (a non-acetylated mannuronic acid decasaccharide; $ManA_{10}$). No acetylesterase activity was observed for $AlgF_{Pp}$ (Figure 5). Addition of $AlgF_{Pp}$ to either $AlgJ_{Pp}$ or $AlgX_{Pp}$ did not increase observed acetylesterase activity, with or without presence of $ManA_{10}$ (Figure 5). Similarly, addition of $AlgF_{Pp}$ to a combination of $AlgJ_{Pp}$ and $AlgX_{Pp}$ did not result in an increase acetyltransferase activity, with or without presence of $ManA_{10}$, suggesting that the presence of AlgF does not influence overall acetylesterase activity. Therefore, the proposed formation of an acetylation machinery complex, although required for alginate acetylation *in vivo*, does not affect the acetylesterase activity of AlgJ or AlgX *in vitro*.

Even though $AlgF_{Pp}$ demonstrated a lack of acetylesterase activity, some of the AlgF-related ß-sandwich proteins bind sugars/small molecules. Thus, the ability of $AlgF_{Pa}$ to bind carbohydrate polymer was investigated using an electrospray ionization mass spectrometry (ESI-MS) binding assay. Nine

mannuronic acid oligomers ranging from 4 to 12 sugars in length ($ManA_4$ to $ManA_{12}$) were tested. $AlgF_{Pa}$ did not display any affinity for the oligomers tested. The approximate K_a values measured were less than 500 M^{-1} for all oligomers tested (Table S1). This is similar to what was observed previously for AlgJ (20). In contrast, AlgX binds to mannuronic acid oligomers in a length dependent manner (20). As the data suggest that AlgF does not bind alginate in isolation, it most likely functions as a protein-protein interaction mediator between AlgJ and AlgX.

AlgIJFX form a complex in P. aeruginosa

The *in vitro* binding data obtained by ITC suggests that AlgF interacts with AlgX and AlgJ, and that AlgF may mediate the formation of a complex when all three proteins are present. To examine whether these findings also hold true in *P. aeruginosa*, we performed co-immunoprecipitation (co-IP) experiments from lysed *P. aeruginosa* cells expressing vesicular stomatitis virus glycoprotein (VSV-G) tagged AlgX, AlgJ, or AlgF. The VSV-G sequence was introduced at the C-terminus of each gene directly on the chromosome of PAO1 Δ*wspF* P_{BAD}*alg* (46). In this strain, the native *algD* promoter has been replaced by *araC*-P_{BAD}, allowing for high level inducible expression of the *algD* operon in the presence of arabinose. Clarified lysates were applied to agarose resin conjugated to anti-VSV-G monoclonal antibodies, and the elution from the resin after washing was analyzed by Western blot using protein-specific polyclonal antibodies. The corresponding untagged protein was used as a negative binding control. When $AlgX_{Pa}^{C\text{-}VSV\text{-}G}$ was supplied as the bait, $AlgF_{Pa}$ was identified as an interaction partner (Figure 6A). $AlgF_{Pa}$ was not identified in the elution from the negative control, indicating that the observed interaction is not due to non-specific binding with the co-IP resin (Figure 6A). To confirm this finding, co-IP eluates from six independent co-IP experiments using $AlgX_{Pa}^{C\text{-}VSV\text{-}G}$ as the bait were analyzed by ESI-MS. $AlgF_{Pa}$, as well as the previously identified interaction partner $AlgK_{Pa}$ (47, 48), were significantly enriched in the $AlgX_{Pa}^{C\text{-}VSV\text{-}G}$ eluate versus the untagged negative control (Figure 6B), confirming the interaction between $AlgX_{Pa}$ and $AlgF_{Pa}$. When $AlgF_{Pa}^{C\text{-}VSV\text{-}G}$ was supplied as the bait, no co-eluting proteins were identified

suggesting that addition of the VSV-G tag to $AlgF_{Pa}$ may have disrupted the stability or function of $AlgF_{Pa}$.

Co-IP could not be performed successfully with $AlgI_{Pa}$ as the bait due to the instability and aggregation of $AlgI_{Pa}$ after solubilization from *P. aeruginosa* membranes. Attempts to optimize extraction using various detergents were unsuccessful, precluding the ability to generate an $AlgI_{Pa}$-specific polyclonal antibody. While we were able to generate a VSV-G-tagged construct of $AlgI_{Pa}$ that could complement acetylation in an *algI* deletion mutant, $AlgI_{Pa}$ also aggregates in Laemmli buffer under all conditions tested, preventing its detection by Western blot. To determine whether the destabilization of $AlgI_{Pa}$ during the detergent extraction step of co-IP experiments would have an effect on the stability of other acetylation proteins, a mutual stability analysis was performed using a Δ*algI* variant to mimic the loss of $AlgI_{Pa}$ due to detergent extraction-mediated aggregation. When expression of $AlgJ_{Pa}$ was analyzed by Western blot, a significant reduction in steady-state protein levels was observed in the Δ*algI* background versus wild-type (Figure 6C). Complementation of *algI* at the neutral *attTn7* site on the *P. aeruginosa* chromosome restored $AlgJ_{Pa}$ to wild-type levels (Figure 6C), suggesting that the reduction in whole-cell $AlgJ_{Pa}$ levels was due specifically to the deletion of *algI*. Indeed, when co-IP experiments were performed with $AlgJ_{Pa}^{C\text{-}VSV\text{-}G}$ as the bait, no interaction partners were identified, likely due to $AlgI_{Pa}$ aggregation after solubilization of the membranes and the resultant effects on the stability of $AlgJ_{Pa}$. Overall, these data support the presence of a physiological interaction between $AlgX_{Pa}$ and $AlgF_{Pa}$ and imply also that $AlgJ_{Pa}$ and $AlgI_{Pa}$ interact based on the observed stability requirement of $AlgJ_{Pa}$ for $AlgI_{Pa}$.

Predictive modelling of the AlgKXF and AlgIJ complexes

The structure of the $AlgKX_{Pp}$ complex has been previously determined experimentally (PDB: 7ULA) and AlphaFold2 was shown to accurately predict the structure/interaction interface of the $AlgKX_{Pp}$ complex across different *Pseudomonas* species (48). Building on the success of the AlphaFold2 model of $AlgKX_{Pp}$, we next sought to determine whether the program could predict how $AlgF_{Pp}$ may interact with

AlgX$_{Pp}$ and AlgK$_{Pp}$. Using this approach, we were able to generate a high-confidence model of the AlgKXF$_{Pp}$ complex involved in alginate modification and export (Figures 7A and S6). The predicted AlgKXF$_{Pp}$ complex shows that AlgK$_{Pp}$ and AlgX$_{Pp}$ maintain the same interaction interface as previously reported in the experimentally determined structure (48). Analysis of the AlgKXF$_{Pp}$ model by the PISA server (38) suggests that AlgF$_{Pp}$ only interacts with AlgX$_{Pp}$. The modelled AlgXF$_{Pp}$ interaction interface was calculated to have a buried surface area of 1545 Å^2 mediated by 12 hydrogen bonds and six salt bridges (Figure 7B). Most notably, ten out of eleven predicted interacting residues on AlgF$_{Pp}$ interact with AlgX$_{Pp}$ using their side chain atoms and all eleven residues are present on coil regions of AlgF$_{Pp}$. Three AlgF$_{Pp}$ interaction interface residues are present on the N-terminal domain (Asp29 and Tyr33 involved in hydrogen bonding and Lys39 involved in both hydrogen bonding and salt bridge interactions), while the remaining nine are present on the C-terminal domain (Gln123, Lys124, Asn163, Pro164, Lys166, Glu187, Arg187 and Glu190) (Figure 7B). Thus, both the N- and C-terminal domains are predicted to be required for the interaction with AlgX$_{Pp}$. In AlgF$_{Pa}$, these interaction interface residues correspond to Asp29, Tyr34, Lys40, Gln124, Lys125, Asn164, Pro165, Lys167, Ala188, Arg189, and Glu191. Of the nine residues that are present in the AlgF$_{Pa}$ experimentally determined structure, four of these residues are highly conserved, four are conserved, and one is less conserved (Figure 2E). Building on this model, we next attempted to model the AlgKXFJ$_{Pp}$ complex using AlphaFold2. To expand this prediction to include AlgJ$_{Pp}$, due to the 1400 residues limitation in AlphaFold2, we only included the C-terminal region of AlgK$_{Pp}$ that binds to AlgX$_{Pp}$ when predicting the AlgKXFJ$_{Pp}$ complex. Although the predicted models revealed a consistent AlgKXF$_{Pp}$ interaction interface (as shown in Figure 7), the predicted alignment error (PAE) plot revealed the interaction of AlgJ$_{Pp}$ with AlgKFX$_{Pp}$ could not be accurately predicted as the PAE values for AlgJ$_{Pp}$ were estimated to be >25Å (Figure S7). Thus, we were unable to generate a high-confidence model to illustrate how AlgF$_{Pp}$ and AlgJ$_{Pp}$ may interact.

Given that our mutual stability data from *P. aeruginosa* suggests an interaction between AlgI$_{Pa}$ and AlgJ$_{Pa}$, we also used AlphaFold to model the AlgIJ$_{Pp}$ complex. A high-confidence model of the AlgIJ$_{Pp}$ complex was generated for this part of the predicted acetylation complex (Figure S8). This

complex suggests that it is predominantly the transmembrane domain of AlgJ that interacts with AlgI. Analysis by PISA reveals that the interaction interface area between AlgI and AlgJ is 2122 $Å^2$, mediated by ten hydrogen bonds and three salt bridges. The N-terminal helix of AlgJ is inserted into the inner membrane and is predicted to pack between the first and last helices of AlgI (Figure S8).

DISCUSSION

In this study, we present the structure of AlgF and, using *in vitro* studies coupled with analyses from *P. aeruginosa*, establish that the proteins involved in alginate acetylation (AlgI, J, F, and X) interact to form an acetylation complex that is linked to the outer membrane export machinery *via* an interaction between AlgX and AlgK. We found that AlgF consists of two β-sandwich domains joined by a linker, and our functional characterizations suggest that AlgF is unlikely to function as an alginate acetyltransferase as it lacks acetylesterase activity and is unable to bind alginate *in vitro*. Considering that most of its structural neighbours are involved in protein-ligand interactions, we propose that AlgF functions as a protein-protein interaction mediator within the alginate biosynthetic system to coordinate an AlgJFX periplasmic acetylation complex.

A search for AlgF structural homologs using the DALI server revealed proteins involved in ligand binding. The tandem two-domain architecture of AlgF resembles the binding module of the Eukaryotic peptide transporter PepT2, which mediates an interaction between trypsin and the membrane transporter domain (41). This functionality could be mirrored with AlgF localizing and/or strengthening interactions between the acetyltransferase proteins and the rest of the alginate biosynthetic complex. As evidence of this role for AlgF, we have been able to establish that AlgF binds to both AlgX and AlgJ *in vitro*. We originally hypothesized that one domain of AlgF binds AlgJ at the inner membrane while the other binds to AlgX however, structural prediction of the $AlgKXF_{Pa}$ model suggests that both domains are required for its interaction with AlgX. Thus, further binding studies in conjugation with targeted mutagenesis of AlgF are required to ascertain which regions of AlgF are involved in interacting with either AlgX or AlgJ.

Previous studies have demonstrated that alginate is produced but not acetylated when either AlgJ or AlgX enzymatic activity is compromised (19, 20). Taking into consideration all the data presented on AlgJFX thus far, this suggests that transfer of an acetyl group from AlgJ to AlgX occurs and is required for polymer acetylation. As no direct interaction between AlgJ and AlgX was observed in this study, we hypothesize that AlgF is necessary to bring AlgJ and AlgX together in close enough proximity for acetyl relay and that lack of AlgF would decouple the acetyltransferase process. AlgI has also been found to be critical for acetylation of the nascent polymer (18, 21, 23). Our mutual stability studies demonstrate that AlgI may be part of the acetylation complex. This hypothesis is further strengthened by our AlphaFold2 model that suggests that AlgI is linked to the acetylation machinery primarily through the transmembrane domain of AlgJ (45). While we have been unable to model the entire AlgIJFX complex, we propose that AlgIJFX serve as an acetyl relay to transfer an acetate from AlgI, across the inner membrane first to AlgJ, then AlgX and finally to the polymer (Figure 8). Comparably, acetylation of cellulose in *P. fluorescens* requires the proteins WssF/H/I/G which are homologous to the alginate proteins, AlgX/I/J/F (49). The AlgF-like protein, WssG, in acetylated cellulose biosynthesis is poorly characterized and its role remains unknown (49). Future experiments along the same lines as those presented here could help establish whether WssG is also a protein-protein interaction mediator and critical for the formation of a WssH/I/G/F complex.

In addition to the AlgI/J/F/X interactions outlined here, previous studies have demonstrated that AlgX and AlgK form a robust complex that couples alginate acetylation and export (48). Furthermore, given that AlgE localization is dependent on the presence of AlgK (50), formation of an AlgEKX outer membrane secretion complex has also been proposed (48). Within the inner membrane, it has been suggested that Alg8 and Alg44 form a synthase co-polymerase complex (51). Alg44's periplasmic domain has been proposed to interact with AlgX and AlgK (52). These previously established interaction networks highlight the mechanisms required for alginate synthesis. Our ability to observe the well-established

AlgX-AlgK interaction using co-IPs reinforces the results obtained here that link AlgX to AlgF and the rest of the acetylation machinery. The interactions between the periplasmic acetylation proteins have been found to be relatively weak by ITC with μM affinities. Thus, it may be possible that this weak binding is an artifact of *in vitro* protein studies of binary rather than native multi-protein interactions. The acetylation proteins may interact with a higher affinity once the rest of the biosynthetic complex and alginate substrate is present, allowing for a more stable complex *in vivo*. This hypothesis is not without precedent in large protein complexes (53–55). Specifically, the VirB type IV secretion system complex functions as a minimal set of VirB7 to VirB10 proteins, while the addition of VirB1 to VirB4 increases the activity of the transport complex dramatically, as well as increases the abundance of macrocomplex protein interactions (54). Weak μM interactions between proteins may also indicate the presence of a transient overall biosynthetic complex (55), where a number of subcomplexes may be present in the alginate biosynthesis pathway with variable intra- and inter-subcomplex affinities. Neither high affinity interactions nor stable complex formation may be needed (or desirable) in order to fine-tune alginate modification, as the degree of acetylation is seen to vary depending on bacterial strain and species or on growth conditions and may even vary over the course of biofilm development, maintenance, and dispersal (56–59). If this is the case, then structural determination of subcomplexes with the alginate biosynthetic system may be more reasonable and realistic compared to determination of the complex in its entirety.

The structural determination of AlgF, structural homology searches, and characterization of protein function have enabled us to identify that AlgF mediates protein-protein interactions in the alginate acetylation machinery. The formation of an AlgIJFX acetylation complex supports the previously proposed relay mechanism for alginate modification where AlgF mediates interactions between AlgJ and AlgX for acetylation of the polymer (18–20). For the first time, we are able to build upon established protein networks described above and show links from the inner membrane complex AlgI/J to AlgX/K at the outer membrane. These complexes are linked via AlgF and join the modification subcomplex in the inner membrane/periplasm with the outer membrane export subcomplex. These data are suggestive of a

large protein interaction network and support the hypothesis of a trans-envelope macrocomplex encompassing all of the exopolysaccharide biosynthetic proteins (18, 60). Furthermore, recent studies on the homologous cellulose biosynthetic machinery have shown the presence of an inner membrane subcomplex formed by cytoplasmic, transmembrane, and periplasmic proteins (61–64). Future work with alginate proteins may uncover similar interactions with cytoplasmic components including sugar precursor enzymes, thus expanding our knowledge of how alginate polymerization and precursor biosynthesis may be coupled. Understanding the biosynthesis of exopolysaccharides, including the alginate system, will require further studies of the protein interaction networks not only at a protein-protein level but also at a cellular level. The results presented here provide the first insight into a membrane-spanning polysaccharide secretion complex with significant etiological consequences for patient outcomes in cystic fibrosis.

METHODS

Bacterial strains, plasmids, and growth conditions

A detailed list of the bacterial strains and plasmids used in this study can be found in Table S2. All *P. aeruginosa* mutant and complemented strains were derived from PAO1 (65) and were constructed using allelic exchange and miniTn7 mutagenesis (66, 67), as described below. Unless otherwise stated, lysogeny broth (LB) was used for growth of all strains. LB contained, per litre of ultrapure water, 10 g tryptone, 5 g NaCl, and 10 g yeast extract. Vogel-Bonner minimal medium (VBMM) was prepared as a 10× concentrate containing, per litre of ultrapure water, 2 g $MgSO_4 \cdot 7H_2O$, 20 g citric acid, 100 g K_2HPO_4, and 35 g NH_4HPO_4, and was diluted to 1× as needed. To prepare solid media, 1.5% (w/v) agar were added to LB or VBMM. Where appropriate, antibiotics were added to growth media. For *E. coli*, 10 µg/ml gentamicin, 100 µg/ml carbenicillin, or 50 µg/ml kanamycin was used. For *P. aeruginosa*, 30 or 60 µg/ml gentamicin was used depending on the application, as described below.

P. aeruginosa and P. putida gene expression in E. coli

The nucleotide sequences of AlgF from *P. aeruginosa* PAO1 and *P. putida* KT2440, and of AlgX from *P. putida* KT2440 were obtained from the *Pseudomonas* Genome Database (25). $AlgF_{Pa}^{30-216}$ and $AlgF_{Pp}^{29-215}$ were PCR amplified from genomic DNA. Primer sequences are as indicated in Table S3. Primers account for entire full-length proteins without the respective N-terminal signal sequence as predicted by SignalP (68) and introduce *Nde*I and *Xho*I restriction sites. The codon-optimized gene for expression in *E. coli* of full-length $AlgX_{Pp}$ included flanking *Nde*I and *Xho*I restriction sites at the 5' and 3' ends, respectively, was synthesized by BioBasic. $AlgF_{Pa}^{30-216}$ and codon-optimized $AlgX_{Pp}$ were incorporated into the pET24b vector for C-terminal His_6-tag protein expression. $AlgF_{Pp}^{29-215}$ was incorporated into the pET28a vector with a 3' stop codon for N-terminal His_6-tag protein expression. For each protein construct, *E. coli* BL21 CodonPlus (λDE3) cells (Stratagene) were transformed with expression vector and grown in LB broth containing 50 μg/ml kanamycin at 37 °C. Once the OD600 of the culture reached 0.6, protein expression was induced by the addition of IPTG to a final concentration of 1 mM. The cell culture was incubated at 18 °C for 16 h prior to being harvested by centrifugation at 6700 × *g* for 25 min at 4 °C. Cell pellets were stored until needed at -20 °C. $AlgJ_{Pa}^{79-379}$ and $AlgJ_{Pp}^{75-370}$ were expressed as described previously (20).

Purification of His_6-tagged protein

The cell pellet from 1 L of bacterial culture was thawed and resuspended in 50 mL of lysis buffer (50 mM Tris pH 8.0, 500 mM NaCl, 0.5 M EDTA, 1 mM DTT, 1 mM PMSF, 2% (v/v) glycerol, 1 mg/mL lysozyme) with one Roche Complete protease-inhibitor cocktail (EDTA-free) tablet. The resuspended pellet was incubated at 4 °C for 30 min. Cells were homogenized at 15000 psi using an Emulsiflex C3 (Avestin Inc.) for 3 passes or until fully lysed. Cell lysate was centrifuged at 20100 × *g* for 20 min at 4 °C to remove cellular debris. The resultant lysate supernatant was loaded onto Ni-NTA resin and washed with 30 column volumes of 50 mM Tris pH 8.0, 500 mM NaCl, 2% (v/v) glycerol, and 30 mM imidazole. Protein was eluted using similar buffer with 300 mM imidazole and concentrated by centrifugation with 4 kDa (AlgF) or 30 kDa (AlgJ and AlgX) cutoff Vivaspin Turbo centrifugal concentrators (Sartorius). His_6-

tagged protein was further purified using a HiLoad 16/60 Superdex 200 prep-grade size exclusion column (GE Healthcare) in 50 mM Tris pH 7.5, 500 mM NaCl, and 2% (v/v) glycerol. Protein purification was monitored throughout by SDS-PAGE. $AlgJ_{Pp}$ and $AlgX_{Pp}$ proteins were purified as described previously (20, 69).

NMR structure determination

NMR studies on $^{1}H,^{15}N,^{13}C$ $AlgF_{Pa}^{30-216}$ were carried out at a protein concentration of 1 mM in 50 mM phosphate buffer pH 6.8, 10 mM DTT, 2% (v/v) glycerol, 10% D_2O. To produce uniformly labeled protein, cells were grown in minimal media supplemented with 1 g of ^{15}N-NH_4Cl and 2 g of ^{13}C-glucose per litre, and the protein was expressed and purified as described above. The NMR spectra were collected at QANUC on either a Varian INOVA 500 MHz or 800 MHz NMR spectrometer with triple resonance cryoprobes. Backbone resonances were assigned using HNCACB, CBCA(CO)NH, HNCA, and HNCO triple resonance experiments and side-chain resonances were assigned using CCC-TOCSY, HCC-TOCSY and CT-HSQC experiments (31). N- and C-NOESY-HSQC (both aliphatic and aromatic) were used to obtain NOE distance restraints for structural determination purposes. Data were processed with NMRPipe and visualized with NMRDraw (29). Spectral analysis was performed with either NMRView (28, 30) or Analysis by CcpNmr (32, 33). Structures were calculated using CYANA (27) and with the CS-Rosetta server (26), and the models were visualized using PyMOL (The PyMOL Molecular Graphics System, Version 1.2, Schrödinger, LLC). NOE derived models were compared to restraints using the Protein Structure Validation Suite (35) and the Analysis integrated RPF protocol (PyRPF) (32, 33). The CS-Rosetta determined ensembles of the N- and C-terminal domains have been deposited in the PDB with accession codes 6CZT and 6D10 respectively. Relevant NMR data has been deposited in the Biological Magnetic Resonance Bank (BMRB), accession code 30450.

Structure analysis tools

Inter-residue contacts were determined by CMview (34) and visualized in Excel. Conservation analysis

was performed using the ConSurf server with their automatically generated homolog search and multiple sequence alignment (37). Coulombic surface potentials were calculated in ChimeraX (70). Structures were visualized in PyMol and ChimeraX. A tertiary structure comparison search was conducted using the DALI server for the CYANA-determined AlgF N- and C-terminal domains (39).

Acetylesterase activity assay

Reactions were carried out as previously described (19, 20). Briefly, reactions contained 5 μM of each protein ($AlgJ_{Pa}^{79-379}$, $AlgF_{Pa}^{30-216}$, $AlgX_{Pa}$) in 50 mM sodium HEPES pH 7.6 and 75 mM NaCl at 25 °C and were initiated with the addition of 3-carboxyumbelliferyl acetate (ACC) to 2 mM (dissolved in DMSO at stock concentrations of 20 mM). Deacetylated poly-mannuronate was prepared from *P. aeruginosa* FRD462 as previously described (71) and added at a concentration of 1 mg/mL. The final concentration of DMSO in each reaction was 2% (v/v). Hydrolysis was measured by fluorescence for 20 min with an excitation and emission wavelength of 386 and 446 nm, respectively (72). Reaction rates were calculated using a calibration curve for 7-hydroxycoumarin-3-carboxylic acid, the fluorescent hydrolysis product of ACC. Background hydrolysis rates were measured and subtracted from reaction rates. Assays were carried out in triplicate in 96-well microtitre plates and measured using a SpectraMax M2 microplate reader (Molecular Devices, Sunnyvale, CA). Data analysis was carried out in Prism 7 (Graph Pad) and statistical analyses were performed using an ordinary one-way ANOVA.

Alginate binding assay

Assays were performed as previously described (20) with a range of synthesized oligomannuronic acid oligomers (73).

Isothermal titration calorimetry (ITC)

P. putida protein constructs were used for ITC analyses. ITC experiments were performed with a MicroCal Auto-ITC200 (Malvern) in a buffer consisting of 50 mM Tris pH 7.8, 150 mM NaCl, 2% (v/v)

glycerol, 50 mM arginine, and 50 mM glutamic acid at 20 °C. The Arg/Glu buffer components were used to reach the higher protein concentrations required for ITC experiments (74). ITC mixtures included: 1.86 mM AlgJ (syringe) titrated into 188 µM AlgF (cell) for AlgJ:AlgF; 4.17 mM AlgF (syringe) titrated into 500 µM AlgX (cell) for AlgF:AlgX; 2.97 mM AlgJ (syringe) titrated into 170 µM AlgX (cell) for AlgJ:AlgX. AlgX was placed in the cell due to a lower yield of protein. Runs were performed using 16-20 2.5 µL injections at an interval of 240 s. Data were analyzed using MicroCal Origin ITC Analysis software (Malvern).

P. aeruginosa strain construction

In-frame, unmarked *algJ* and *algI* gene deletions in *P. aeruginosa* PAO1 Δ*wspF* P_{BAD}*alg* (46) were generated using an established allelic replacement protocol (66). Construction of the gene deletion alleles was performed by amplifying flanking regions of the *algJ* or *algI* open reading frames (ORFs) and joining these flanking regions by splicing-by-overlap extension PCR (primers are listed in Table S3). The upstream forward and downstream reverse primers were tailed with EcoRI and HindIII restriction sequences, respectively, and the assembled Δ*algJ* and Δ*algI* alleles were cloned into pEX18Gm. The resulting allelic exchange vectors, pEX18Gm::Δ*algJ* and pEX18Gm::Δ*algI*, were selected on LB agar containing 10 µg/mL gentamicin and verified by Sanger sequencing using the M13F and M13R primers (Table S3).

The deletion alleles encoded by pEX18Gm::Δ*algJ* and pEX18Gm::Δ*algI* were introduced into *P. aeruginosa* PAO1 Δ*wspF* P_{BAD}*alg* via biparental mating with the donor strain *E. coli* SM10 (75). Merodiploids were selected on VBMM agar containing 60 µg/mL gentamicin. SacB-mediated counter selection was carried out to select for double cross-over mutations on no-salt lysogeny broth agar containing 15% (w/v) sucrose. Unmarked gene deletions were identified by colony PCR using primers that targeted the outside, flanking regions of *algJ* or *algI* (Table S3). These PCR products were Sanger sequenced using the same primers to confirm the correct deletion.

Construction of strains encoding C-terminally VSV-G-tagged AlgJ, AlgF, and AlgX was performed as above, with the following modifications. The upstream and downstream regions flanking the stop codon of *algX*, *algJ*, and *algF* were amplified using primer pairs whose upstream reverse and downstream forward primers were tailed with complementary sequence encoding the VSV-G peptide sequence (Table S3). The VSV-G sequence was encoded upstream of the stop codon for each gene. The flanking upstream and downstream PCR products were then assembled by splicing-by-overlap extension PCR and cloned into pEX18Gm using SacI and HindIII restriction sites for AlgX and AlgJ, and EcoRI and HindIII restriction sites for AlgF.

miniTn7 complementation

For gene complementation in *P. aeruginosa*, pUC18T-miniTn7T-Gm, which allows for single-copy chromosomal insertion of genes (76), was modified to allow for arabinose-dependent expression of complemented genes. The *araC*-P_{BAD} promoter from pJJH187 (77) was amplified using the primer pair miniTn7 pBAD F and miniTn7 pBAD R, the latter of which contains flanking sequence encoding SmaI, NotI, PstI, and NcoI sites to generate a multiple cloning site downstream of the *araC*-P_{BAD} promoter (Table 3). The resulting PCR product was cloned into the SacI and HindIII sites of pUC18T-miniTn7T-Gm to generate pUC18T-miniTn7T-Gm-pBAD (Table S2).

The ORF corresponding to *algJ* and *algI* was amplified using the primer pairs AlgJ miniTn7 F + AlgJ miniTn7 R, and AlgI miniTn7 F + AlgI miniTn7 R, respectively, which encode a synthetic ribosome binding site upstream of the start codon (Table S3). The resultant PCR products were cloned into pUC18T-miniTn7T-Gm-pBAD using the NcoI + SacI and NotI + NcoI sites, respectively, selected on LB agar containing 10 μg/mL gentamicin and 100 μg/mL carbenicillin, and confirmed by Sanger sequencing using the miniTn7 SeqF and miniTn7 SeqR primers (Table S3).

Complemented *P. aeruginosa* strains were generated through incorporation of miniTn7 vectors at the neutral *attTn7* site on the *P. aeruginosa* chromosome via electroporation of miniTn7 vectors, along with the helper plasmid pTNS2, as previously described (67). Transposon mutants were selected on LB agar containing 30 µg/ml gentamicin.

Co-immunoprecipitation (Co-IP)

1 L of LB, containing 0.5% (w/v) L-arabinose and 30 µg/mL gentamicin, was inoculated with a *P. aeruginosa* strain carrying a VSV-G-tagged alginate protein and allowed to grow overnight at 37 °C with shaking. The next day, cells were collected at 5,000 × *g* for 20 min at 4 °C, resuspended in 50 mL of lysis buffer (20 mM Tris pH 8.0, 100 mM NaCl, 1 mM EDTA, 1 mg/mL lysozyme, 100 µg/mL DNase I, 2% (w/v) Triton X-100, 1 SIGMAFAST EDTA-free protease inhibitor cocktail tablet), and rocked for 2 h at 4 °C to allow for cell lysis. The cell lysate was subsequently clarified by centrifugation at 30,000 × *g* for 30 min at 4 °C. A sample of the clarified whole cell lysate was collected before application to the IP resin as a representative example of the input into the experiment. The IP resin (Sigma anti-VSV-G monoclonal antibody-agarose) was prepared by mixing 60 µL of slurry with 10 ml of wash buffer (20 mM Tris pH 8.0, 100 mM NaCl, 2% (w/v) Triton X-100), followed by collection of the IP resin by centrifugation at 100 × *g* for 2 min at 4 °C and removal of the supernatant. The clarified cell lysate was applied to the washed IP resin and incubated at 4 °C for 1 h with agitation. The IP resin was then collected by centrifugation at 100 × *g* for 2 min at 4 °C and the supernatant discarded. The resin was washed four times with 10 ml of wash buffer as above, followed by one wash with 10 mL of detergent-free wash buffer (20 mM Tris pH 8.0, 100 mM NaCl) to remove non-specifically bound protein. Protein was then eluted from the resin by incubation in 110 µL of 0.2 M glycine, pH 2.2, for 15 min at room temperature, followed by collection of the resin by centrifugation at 100 × *g* for 2 min at 4 °C and removal of the supernatant containing eluted protein. The eluate was then neutralized by the addition of 40 µl of 1 M K_2HPO_4. Samples of the eluate were analyzed by ESI-MS by the SPARC Biocentre (The Hospital for Sick Children). For Western blot analysis, equal volumes of eluate and 2× Laemmli buffer were mixed,

heated at 95 °C for 10 min, and separated by SDS-PAGE followed by Western blot as described below. As a negative control, an IP experiment was also performed using a *P. aeruginosa* strain expressing the corresponding untagged alginate protein.

Western blot sample preparation and analysis

To analyze protein levels from alginate-overproducing *P. aeruginosa* strains, 5 ml of LB containing 0.5% (w/v) L-arabinose was inoculated with the appropriate strain and allowed to grow overnight at 37 °C with shaking. The next day, culture density was normalized to an OD_{600} = 1 and 1 mL of the resulting culture was centrifuged at 5,000 × *g* for 5 min to pellet cells. The cell pellet was resuspended in 100 µL of 2× Laemmli buffer, heated for 10 min at 95 °C and analyzed by SDS-PAGE followed by Western blot.

For Western blot analysis, a 0.2 µm polyvinylidene difluoride (PVDF) membrane was wetted in methanol and soaked for 5 min in Western transfer buffer (25 mM Tris-HCl, 150 mM glycine, 20% (v/v) methanol) along with the SDS-PAGE gel to be analyzed. Protein was transferred from the SDS-PAGE gel to the PVDF membrane by wet blotting (25 mV, 2 h). The membrane was briefly rinsed in Tris-buffered saline (10 mM Tris-HCl pH 7.5, 150 mM NaCl) containing 0.5% (v/v) Tween-20 (TBS-T) before blocking in 5% (w/v) skim milk powder in TBS-T for 2 h at room temperature with gentle agitation. The membrane was briefly washed again in TBS-T before incubation overnight with primary antibody (1:1,000 α-AlgJ, 1:250 α-AlgF, 1:1,000 α-AlgX, 1:3,000 α-PilP; described below) in TBS-T with 1% (w/v) skim milk powder at 4 °C. The next day, the membrane was washed four times in TBS-T for 5 min each before incubation for 1 h with secondary antibody (1:2,000 dilution of BioRad affinity purified goat α-rabbit IgG conjugated to alkaline phosphatase) in TBS-T with 1% (w/v) skim milk powder. The membrane was then washed three times with TBS-T for 5 min each before development with 5-bromo-4-chloro-3-indolyl phosphate/nitro blue tetrazolium chloride (BioShop ready-to-use BCIP/NBT solution). Developed blots were imaged using a BioRad ChemiDoc imaging system.

Antibody production and purification

PilP and AlgX antisera were generated and purified as described previously (19, 78). $AlgF_{Pa}^{30-216}$ and $AlgJ_{Pa}^{79-379}$ were purified as described above and used to generate antiserum from rabbits via a standard 70 day protocol (Cedarlane Laboratories). The α-AlgF and α-AlgJ antibodies were further purified using a protocol adapted from Salamitou *et al.* (79). Briefly, 200 µg of purified $AlgF_{Pa}^{30-216}$ or $AlgJ_{Pa}^{79-379}$ were loaded on a 16% or 12% Tris-HCl polyacrylamide gel, respectively and transferred to a PVDF membrane. The membrane was stained with Ponceau S and the band corresponding to $AlgF_{Pa}^{30-216}$ or $AlgJ_{Pa}^{79-379}$ was cut out and blocked using PBS pH 7.0 with 0.1% (w/v) Tween 20 and 5% (w/v) skim milk powder for 1 h. The membrane was then incubated with α-AlgF or α-AlgJ antisera overnight at 4 °C followed by incubation at room temperature for 2 h. After washing in PBS, α-AlgF or α-AlgJ antibodies were eluted from the membrane by incubation in 700 µL of 0.2 M glycine pH 2.2 for 15 min, followed by neutralization with 300 µL of 1 M K_2HPO_4. The purified antibodies were dialyzed overnight against PBS, mixed 1:1 with glycerol, and stored at -20 °C. α-AlgF antibodies were used at a dilution of 1:250, α-AlgJ antibodies were used at a dilution of 1:1,000, α-AlgX antibodies were used at a dilution of 1:1,000, and anti-PilP antibodies were used at a dilution of 1:3,000.

AlphaFold modelling

AlphaFold predictions were run using ColabFold v 1.5.2 with default parameters (i.e. alphafold2_multimer_v3). No template information was used. and the multiple sequence alignment options chosen were mmseq2_uniref_env and unpaired_paired. Five structures for each complex were predicted and used without relaxation using Amber. The sequences for *P. putida* were retrieve from UniProt accession numbers (AlgI: Q88ND2 AlgJ: Q88ND3; AlgF: Q88ND4; AlgX: Q88ND0; AlgK: Q88NC7) were used either as is (AlgI, AlgJ) or with their signal sequences (as determined by SignalP (68)) removed (AlgF, AlgX, and AlgK).

Software support

620 The majority of software programs used in this report were configured and supported by the SBGrid
621 consortium (80).

622

623 **REFERENCES**

624 1. Erskine, E., Morris, R. J., Schor, M., Earl, C., Gillespie, R. M. C., Bromley, K. M.,
625 Sukhodub, T., Clark, L., Fyfe, P. K., Serpell, L. C., Stanley-Wall, N. R., and MacPhee, C.
626 E. (2018) Formation of functional, non-amyloidogenic fibres by recombinant *Bacillus*
627 *subtilis* TasA. *Mol Microbiol*. **110**, 897–913
628 2. Flemming, H. C., and Wingender, J. (2010) The biofilm matrix. *Nat Rev Microbiol*. **8**,
629 623–633
630 3. Turnbull, L., Toyofuku, M., Hynen, A. L., Kurosawa, M., Pessi, G., Petty, N. K., Osvath,
631 S. R., Cárcamo-Oyarce, G., Gloag, E. S., Shimoni, R., Omasits, U., Ito, S., Yap, X.,
632 Monahan, L. G., Cavaliere, R., Ahrens, C. H., Charles, I. G., Nomura, N., Eberl, L., and
633 Whitchurch, C. B. (2016) Explosive cell lysis as a mechanism for the biogenesis of
634 bacterial membrane vesicles and biofilms. *Nat Commun*. 10.1038/ncomms11220
635 4. Boisvert, A. A., Cheng, M. P., Sheppard, D. C., and Nguyen, D. (2016) Microbial biofilms
636 in pulmonary and critical care diseases. *Ann Am Thorac Soc*. **13**, 1615–1623
637 5. McKay, G., and Nguyen, D. (2017) *Handbook of Antimicrobial Resistance* (Gotte, M.,
638 Berghuis, A., Matlashewski, G., Wainberg, M. A., and Sheppard, D. C. eds), Springer US
639 6. Whitfield, G. B., Marmont, L. S., and Howell, P. L. (2015) Enzymatic modifications of
640 exopolysaccharides enhance bacterial persistence. *Front Microbiol*. **6**, 1–21
641 7. Forman, S., Bobrov, A. G., Kirillina, O., Craig, S. K., Abney, J., Fetherston, J. D., and
642 Perry, R. D. (2006) Identification of critical amino acid residues in the plague biofilm
643 Hms proteins. *Microbiology (N Y)*. **152**, 3399–3410
644 8. Cerca, N., Jefferson, K. K., Maira-Litrán, T., Pier, D. B., Kelly-Quintos, C., Goldmann, D.
645 A., Azeredo, J., and Pier, G. B. (2007) Molecular basis for preferential protective efficacy
646 of antibodies directed to the poorly acetylated form of staphylococcal poly-N-acetyl-β-(1-
647 6)- glucosamine. *Infect Immun*. **75**, 3406–3413
648 9. Vuong, C., Kocianova, S., Voyich, J. M., Yao, Y., Fischer, E. R., DeLeo, F. R., and Otto,
649 M. (2004) A crucial role for exopolysaccharide modification in bacterial biofilm
650 formation, immune evasion, and virulence. *Journal of Biological Chemistry*. **279**, 54881–
651 54886
652 10. Itoh, Y., Rice, J. D., Goller, C., Pannuri, A., Taylor, J., Meisner, J., Beveridge, T. J.,
653 Preston, J. F., and Romeo, T. (2008) Roles of pgaABCD genes in synthesis, modification,
654 and export of the *Escherichia coli* biofilm adhesin poly-β-1,6-N-acetyl-D-glucosamine. *J*
655 *Bacteriol*. **190**, 3670–3680
656 11. Fong, J. C. N., Syed, K. A., Klose, K. E., and Yildiz, F. H. (2010) Role of Vibrio
657 polysaccharide (vps) genes in VPS production, biofilm formation and *Vibrio cholerae*
658 pathogenesis. *Microbiology (N Y)*. **156**, 2757–2769
659 12. Spiers, A. J., Bohannon, J., Gehrig, S. M., and Rainey, P. B. (2003) Biofilm formation at
660 the air-liquid interface by the *Pseudomonas fluorescens* SBW25 wrinkly spreader requires
661 an acetylated form of cellulose. *Mol Microbiol*. **50**, 15–27

13. Tielen, P., Strathmann, M., Jaeger, K. E., Flemming, H. C., and Wingender, J. (2005) Alginate acetylation influences initial surface colonization by mucoid *Pseudomonas aeruginosa*. *Microbiol Res*. **160**, 165–176
14. Nivens, D. E., Ohman, D. E., Williams, J., and Franklin, M. J. (2001) Role of alginate and its O acetylation in formation of *Pseudomonas aeruginosa* microcolonies and biofilms. *J Bacteriol*. **183**, 1047–1057
15. Farrell, E. K., and Tipton, P. A. (2012) Functional Characterization of AlgL, an Alginate Lyase from *Pseudomonas aeruginosa*. *Biochemistry*. **51**, 255–262
16. Pier, G. B., Coleman, F., Grout, M., Franklin, M., and Ohman, D. E. (2001) Role of alginate O acetylation in resistance of mucoid *Pseudomonas aeruginosa* to opsonic phagocytosis. *Infect Immun*. **69**, 1895–1901
17. Learn, D. B., Brestel, E. P., and Seetharama, S. (1987) Hypochlorite Scavenging by *Pseudomonas aeruginosa* Alginate. *Infect Immun*. **55**, 1813–1818.
18. Franklin, M. J., and Ohman, D. E. (2002) Mutant analysis and cellular localization of the AlgI, AlgJ, and AlgF proteins required for O acetylation of alginate in *Pseudomonas aeruginosa*. *J Bacteriol*. **184**, 3000–3007
19. Riley, L. M., Weadge, J. T., Baker, P., Robinson, H., Codée, J. D. C., Tipton, P. A., Ohman, D. E., and Howell, P. L. (2013) Structural and functional characterization of *Pseudomonas aeruginosa* AlgX: Role of AlgX in alginate acetylation. *Journal of Biological Chemistry*. **288**, 22299–22314
20. Baker, P., Ricer, T., Moynihan, P. J., Kitova, E. N., Walvoort, M. T. C., Little, D. J., Whitney, J. C., Dawson, K., Weadge, J. T., Robinson, H., Ohman, D. E., Codée, J. D. C., Klassen, J. S., Clarke, A. J., and Howell, P. L. (2014) *P. aeruginosa* SGNH Hydrolase-Like Proteins AlgJ and AlgX Have Similar Topology but Separate and Distinct Roles in Alginate Acetylation. *PLoS Pathog*. 10.1371/journal.ppat.1004334
21. Franklin, M. J., and Ohman, D. E. (1996) Identification of *algI* and *algI* in the *Pseudomonas aeruginosa* alginate biosynthetic gene cluster which are required for alginate O acetylation. *J Bacteriol*. **178**, 2186–2195
22. Franklin, M. J., and Ohman, D. E. (1993) Identification of *algF* in the alginate biosynthetic gene cluster of *Pseudomonas aeruginosa* which is required for alginate acetylation. *J Bacteriol*. **175**, 5057–5065
23. Franklin, M. J., Douthit, S. A., and McClure, M. A. (2004) Evidence that the *algI*/*algJ* gene cassette, required for O acetylation of *Pseudomonas aeruginosa* alginate, evolved by lateral gene transfer. *J Bacteriol*. **186**, 4759–4773
24. Nerli, S., and Sgourakis, N. G. (2019) CS-ROSETTA, pp. 321–362, 10.1016/bs.mie.2018.07.005
25. Winsor, G. L., Griffiths, E. J., Lo, R., Dhillon, B. K., Shay, J. A., and Brinkman, F. S. L. (2016) Enhanced annotations and features for comparing thousands of Pseudomonas genomes in the Pseudomonas genome database. *Nucleic Acids Res*. **44**, D646–D653
26. Shen, Y., Lange, O., Delaglio, F., Rossi, P., Aramini, J. M., Liu, G., Eletsky, A., Wu, Y., Singarapu, K. K., Lemak, A., Ignatchenko, A., Arrowsmith, C. H., Szyperski, T., Montelione, G. T., Baker, D., and Bax, A. (2008) Consistent blind protein structure generation from NMR chemical shift data. *Proceedings of the National Academy of Sciences*. **105**, 4685–4690
27. Güntert, P. Automated NMR Structure Calculation With CYANA. in *Protein NMR Techniques*, pp. 353–378, Humana Press, New Jersey, 10.1385/1-59259-809-9:353

28. Kirby, N. I., DeRose, E. F., London, R. E., and Mueller, G. A. (2004) NvAssign: protein NMR spectral assignment with NMRView. *Bioinformatics*. **20**, 1201–1203
29. Delaglio, F., Grzesiek, S., Vuister, GeertenW., Zhu, G., Pfeifer, J., and Bax, A. (1995) NMRPipe: A multidimensional spectral processing system based on UNIX pipes. *J Biomol NMR*. 10.1007/BF00197809
30. Varani, G., Chen, Y., and Leeper, T. C. NMR Studies of Protein–Nucleic Acid Interactions. in *Protein NMR Techniques*, pp. 289–312, Humana Press, New Jersey, 10.1385/1-59259-809-9:289
31. Kanelis, V., Forman-Kay, J. D., and Kay, L. E. (2001) Multidimensional NMR Methods for Protein Structure Determination. *IUBMB Life (International Union of Biochemistry and Molecular Biology: Life)*. **52**, 291–302
32. Vranken, W. F., Boucher, W., Stevens, T. J., Fogh, R. H., Pajon, A., Llinas, M., Ulrich, E. L., Markley, J. L., Ionides, J., and Laue, E. D. (2005) The CCPN data model for NMR spectroscopy: Development of a software pipeline. *Proteins: Structure, Function, and Bioinformatics*. **59**, 687–696
33. Skinner, S. P., Goult, B. T., Fogh, R. H., Boucher, W., Stevens, T. J., Laue, E. D., and Vuister, G. W. (2015) Structure calculation, refinement and validation using CcpNmr Analysis. *Acta Crystallogr D Biol Crystallogr*. **71**, 154–61
34. Vehlow, C., Stehr, H., Winkelmann, M., Duarte, J. M., Petzold, L., Dinse, J., and Lappe, M. (2011) CMView: Interactive contact map visualization and analysis. *Bioinformatics*. **27**, 1573–1574
35. Bhattacharya, A., Tejero, R., and Montelione, G. T. (2006) Evaluating protein structures determined by structural genomics consortia. *Proteins: Structure, Function, and Bioinformatics*. **66**, 778–795
36. Jumper, J., Evans, R., Pritzel, A., Green, T., Figurnov, M., Ronneberger, O., Tunyasuvunakool, K., Bates, R., Žídek, A., Potapenko, A., Bridgland, A., Meyer, C., Kohl, S. A. A., Ballard, A. J., Cowie, A., Romera-Paredes, B., Nikolov, S., Jain, R., Adler, J., Back, T., Petersen, S., Reiman, D., Clancy, E., Zielinski, M., Steinegger, M., Pacholska, M., Berghammer, T., Bodenstein, S., Silver, D., Vinyals, O., Senior, A. W., Kavukcuoglu, K., Kohli, P., and Hassabis, D. (2021) Highly accurate protein structure prediction with AlphaFold. *Nature*. **596**, 583–589
37. Ashkenazy, H., Abadi, S., Martz, E., Chay, O., Mayrose, I., Pupko, T., and Ben-Tal, N. (2016) ConSurf 2016: an improved methodology to estimate and visualize evolutionary conservation in macromolecules. *Nucleic Acids Res*. **44**, W344–W350
38. Krissinel, E., and Henrick, K. (2007) Inference of macromolecular assemblies from crystalline state. *J Mol Biol*. **372**, 774–97
39. Holm, L., and Rosenström, P. (2010) Dali server: conservation mapping in 3D. *Nucleic Acids Res*. **38**, W545–W549
40. Holm, L. (2022) Dali server: structural unification of protein families. *Nucleic Acids Res*. **50**, W210–W215
41. Beale, J. H., Parker, J. L., Samsudin, F., Barrett, A. L., Senan, A., Bird, L. E., Scott, D., Owens, R. J., Sansom, M. S. P., Tucker, S. J., Meredith, D., Fowler, P. W., and Newstead, S. (2015) Crystal Structures of the Extracellular Domain from PepT1 and PepT2 Provide Novel Insights into Mammalian Peptide Transport. *Structure*. **23**, 1889–1899

42. Budzik, J. M., Poor, C. B., Faull, K. F., Whitelegge, J. P., He, C., and Schneewind, O. (2009) Intramolecular amide bonds stabilize pili on the surface of bacilli. *Proc Natl Acad Sci U S A*. **106**, 19992–7
43. van Pee, K., Neuhaus, A., D'Imprima, E., Mills, D. J., Kühlbrandt, W., and Yildiz, Ö. (2017) CryoEM structures of membrane pore and prepore complex reveal cytolytic mechanism of Pneumolysin. *Elife*. 10.7554/eLife.23644
44. Loconte, V., Menozzi, I., Ferrari, A., Folli, C., Imbimbo, B. P., Zanotti, G., and Berni, R. (2019) Structure-activity relationships of flurbiprofen analogues as stabilizers of the amyloidogenic protein transthyretin. *J Struct Biol*. **208**, 165–173
45. Chanasit, W., Gonzaga, Z. J. C., and Rehm, B. H. A. (2020) Analysis of the alginate O-acetylation machinery in *Pseudomonas aeruginosa*. *Appl Microbiol Biotechnol*. **104**, 2179–2191
46. Limoli, D. H., Whitfield, G. B., Kitao, T., Ivey, M. L., Howell, P. L., O'Toole, G. A., and Goldberg, B. (2017) *Pseudomonas aeruginosa* Alginate Overproduction Promotes Coexistence with *Staphylococcus aureus* in a Model of Cystic Fibrosis Respiratory Infection. *mBio*. **8**, 1–18
47. Hay, I. D., Schmidt, O., Filitcheva, J., and Rehm, B. H. A. (2012) Identification of a periplasmic AlgK-AlgX-MucD multiprotein complex in *Pseudomonas aeruginosa* involved in biosynthesis and regulation of alginate. *Appl Microbiol Biotechnol*. **93**, 215–227
48. Gheorghita, A. A., Li, Y. E., Kitova, E. N., Bui, D. T., Pfoh, R., Low, K. E., Whit, G. B., Walvoort, M. T. C., Zhang, Q., Codée, J. D. C., Klassen, J. S., and Howell, P. L. (2022) Structure of the AlgKX modification and secretion complex required for alginate production and biofilm attachment in *Pseudomonas aeruginosa*. 10.1038/s41467-022-35131-6
49. Spiers, A. J., Bohannon, J., Gehrig, S. M., and Rainey, P. B. (2003) Biofilm formation at the air-liquid interface by the *Pseudomonas fluorescens* SBW25 wrinkly spreader requires an acetylated form of cellulose. *Mol Microbiol*. **50**, 15–27
50. Keiski, C. L., Harwich, M., Jain, S., Neculai, A. M., Yip, P., Robinson, H., Whitney, J. C., Riley, L., Burrows, L. L., Ohman, D. E., and Howell, P. L. (2010) AlgK Is a TPR-Containing Protein and the Periplasmic Component of a Novel Exopolysaccharide Secretin. *Structure*. **18**, 265–273
51. Oglesby, L. L., Jain, S., and Ohman, D. E. (2008) Membrane topology and roles of *Pseudomonas aeruginosa* Alg8 and Alg44 in alginate polymerization. *Microbiology (N Y)*. **154**, 1605–1615
52. Fata Moradali, M., Donati, I., Sims, I. M., Ghods, S., and Rehm, B. H. A. (2015) Alginate polymerization and modification are linked in *Pseudomonas aeruginosa*. *mBio*. **6**, 1–17
53. Acuner Ozbabacan, S. E., Engin, H. B., Gursoy, A., and Keskin, O. (2011) Transient protein-protein interactions. *Protein Engineering Design and Selection*. **24**, 635–648
54. Liu, Z., and Binns, A. N. (2003) Functional Subsets of the VirB Type IV Transport Complex Proteins Involved in the Capacity of Agrobacterium tumefaciens To Serve as a Recipient in virB -Mediated Conjugal Transfer of Plasmid RSF1010. *J Bacteriol*. **185**, 3259–3269
55. Kastritis, P. L., Moal, I. H., Hwang, H., Weng, Z., Bates, P. A., Bonvin, A. M. J. J., and Janin, J. (2011) A structure-based benchmark for protein-protein binding affinity. *Protein Science*. **20**, 482–491

56. Schürks, N., Wingender, J., Flemming, H.-C., and Mayer, C. (2002) Monomer composition and sequence of alginates from *Pseudomonas aeruginosa*. *Int J Biol Macromol*. **30**, 105–111
57. Skjåk-Bræk, G., Grasdalen, H., and Larsen, B. (1986) Monomer sequence and acetylation pattern in some bacterial alginates. *Carbohydr Res*. **154**, 239–250
58. Pena, C., Hernandez, L., and Galindo, E. (2006) Manipulation of the acetylation degree of *Azotobacter vinelandii* alginate by supplementing the culture medium with 3-(N-morpholino)-propane-sulfonic acid. *Lett Appl Microbiol*. **43**, 200–204
59. Marty, N. (1992) Influence of nutrient media on the chemical composition of the exopolysaccharide from mucoid and non-mucoid *Pseudomonas aeruginosa*. *FEMS Microbiol Lett*. **98**, 35–44
60. Low, K. E., and Howell, P. L. (2018) Gram-negative synthase-dependent exopolysaccharide biosynthetic machines. *Curr Opin Struct Biol*. **53**, 32–44
61. Acheson, J. F., Ho, R., Goularte, N. F., Cegelski, L., and Zimmer, J. (2021) Molecular organization of the *E. coli cellulose* synthase macrocomplex. *Nat Struct Mol Biol*. **28**, 310–318
62. Krasteva, P. V., Bernal-Bayard, J., Travier, L., Martin, F. A., Kaminski, P. A., Karimova, G., Fronzes, R., and Ghigo, J. M. (2017) Insights into the structure and assembly of a bacterial cellulose secretion system. *Nat Commun*. **8**, 25–28
63. Abidi, W., Decossas, M., Torres-Sánchez, L., Puygrenier, L., Létoffé, S., Ghigo, J.-M., and Krasteva, P. V (2022) Bacterial crystalline cellulose secretion via a supramolecular BcsHD scaffold. *Sci Adv*. **8**, eadd1170
64. Abidi, W., Torres-Sánchez, L., Siroy, A., and Krasteva, P. V. (2022) Weaving of bacterial cellulose by the Bcs secretion systems. *FEMS Microbiol Rev*. 10.1093/femsre/fuab051
65. Stover, C. K., Pham, X. Q., Erwin, A. L., Mizoguchi, S. D., Warrener, P., Hickey, M. J., Brinkman, F. S. L., Hufnagle, W. O., Kowallk, D. J., Lagrou, M., Garber, R. L., Goltry, L., Tolentino, E., Westbrock-Wadman, S., Yuan, Y., Brody, L. L., Coulter, S. N., Folger, K. R., Kas, A., Larbig, K., Lim, R., Smith, K., Spencer, D., Wong, G. K. S., Wu, Z., Paulsen, I. T., Relzer, J., Saler, M. H., Hancock, R. E. W., Lory, S., and Olson, M. V. (2000) Complete genome sequence of *Pseudomonas aeruginosa* PAO1, an opportunistic pathogen. *Nature*. **406**, 959–964
66. Hmelo, L. R., Borlee, B. R., Almblad, H., Love, M. E., Randall, T. E., Tseng, B. S., Lin, C., Irie, Y., Storek, K. M., Yang, J. J., Siehnel, R. J., Howell, P. L., Singh, P. K., Tolker-Nielsen, T., Parsek, M. R., Schweizer, H. P., and Harrison, J. J. (2015) Precision-engineering the *Pseudomonas aeruginosa* genome with two-step allelic exchange. *Nat Protoc*. **10**, 1820–1841
67. Choi, K. H., and Schweizer, H. P. (2006) mini-Tn7 insertion in bacteria with single attTn7 sites: Example *Pseudomonas aeruginosa*. *Nat Protoc*. **1**, 153–161
68. Petersen, T. N., Brunak, S., Von Heijne, G., and Nielsen, H. (2011) SignalP 4.0: Discriminating signal peptides from transmembrane regions. *Nat Methods*. **8**, 785–786
69. Weadge, J. T., Yip, P. P., Robinson, H., Arnett, K., Tipton, P. A., and Howell, P. L. (2010) Expression, purification, crystallization and preliminary X-ray analysis of *Pseudomonas aeruginosa* AlgX. *Acta Crystallogr Sect F Struct Biol Cryst Commun*. **66**, 588–591

70. Pettersen, E. F., Goddard, T. D., Huang, C. C., Meng, E. C., Couch, G. S., Croll, T. I., Morris, J. H., and Ferrin, T. E. (2021) UCSF ChimeraX: Structure visualization for researchers, educators, and developers. *Protein Science*. **30**, 70–82
71. Chitnis, C. E., and Ohman, D. E. (1990) Cloning of *Pseudomonas aeruginosa algG*, which controls alginate structure. *J Bacteriol*. **172**, 2894–2900
72. Chibba, A., Poloczek, J., Little, D. J., Howell, P. L., and Nitz, M. (2012) Synthesis and evaluation of inhibitors of *E. coli* PgaB, a polysaccharide de-N-acetylase involved in biofilm formation. *Org Biomol Chem*. **10**, 7103
73. Walvoort, M. T. C., Van Den Elst, H., Plante, O. J., Kröck, L., Seeberger, P. H., Overkleeft, H. S., Van Der Marel, G. A., and Codée, J. D. C. (2012) Automated solid-phase synthesis of β-mannuronic acid alginates. *Angewandte Chemie - International Edition*. **51**, 4393–4396
74. Golovanov, A. P., Hautbergue, G. M., Wilson, S. A., and Lian, L.-Y. (2004) A Simple Method for Improving Protein Solubility and Long-Term Stability. *J Am Chem Soc*. **126**, 8933–8939
75. Hoang, T. T., Karkhoff-Schweizer, R. R., Kutchma, A. J., and Schweizer, H. P. (1998) A broad-host-range Flp-FRT recombination system for site-specific excision of chromosomally-located DNA sequences: application for isolation of unmarked *Pseudomonas aeruginosa* mutants. *Gene*. **212**, 77–86
76. Choi, K. H., Gaynor, J. B., White, K. G., Lopez, C., Bosio, C. M., Karkhoff-Schweizer, R. A. R., and Schweizer, H. P. (2005) A Tn7-based broad-range bacterial cloning and expression system. *Nat Methods*. **2**, 443–448
77. Almblad, H., Harrison, J. J., Rybtke, M., Groizeleau, J., Givskov, M., Parsek, M. R., and Tolker-Nielsen, T. (2015) The cyclic AMP-Vfr signaling pathway in *Pseudomonas aeruginosa* is inhibited by cyclic Di-GMP. *J Bacteriol*. **197**, 2190–2200
78. Ayers, M., Sampaleanu, L. M., Tammam, S., Koo, J., Harvey, H., Howell, P. L., and Burrows, L. L. (2009) PilM/N/O/P Proteins Form an Inner Membrane Complex That Affects the Stability of the *Pseudomonas aeruginosa* Type IV Pilus Secretin. *J Mol Biol*. **394**, 128–142
79. Salamitou, S., Lemaire, M., Fujino, T., Ohayon, H., Gounon, P., Béguin, P., and Aubert, J. P. (1994) Subcellular localization of *Clostridium thermocellum* ORF3p, a protein carrying a receptor for the docking sequence borne by the catalytic components of the cellulosome. *J Bacteriol*. **176**, 2828–2834
80. Morin, A., Eisenbraun, B., Key, J., Sanschagrin, P. C., Timony, M. A., Ottaviano, M., and Sliz, P. (2013) Collaboration gets the most out of software. *Elife*. 10.7554/eLife.01456

Acknowledgements

Thanks to Patrick Yip, Gaelen Moore, Jeffrey Lynham, Tyler Ricer, and Robert Vernon for technical support and to Perrin Baker for helpful discussion. Thanks to Brookhaven National Laboratory NSLS-II 16-ID beamline staff for technical support and helpful discussion. The acetylesterase pseudosubstrate 3-carboxyumbelliferyl acetate (ACC) was generously donated by Mark Nitz. This research was supported by the Canadian Institutes of Health Research (#MOP-13337, PJT-153322, and FDN-154327). GBW was supported by graduate scholarships from NSERC Canada Graduate Scholarships and Cystic Fibrosis Canada. AAG was supported by graduate scholarship from The SickKids Foundation (RESTRACOMP) and Cystic Fibrosis Canada. YEL was supported by the GlycoNet Summer Awards Program for Undergraduates. JTW was supported by a Postdoctoral Fellowship from NSERC. PLH is the recipient of a Tier I Canada Research Chair. The studies described herein used equipment in the Structural and Biophysical Core Facility at The Hospital for Sick Children, which is funded in part by the Canadian Foundation for Innovation.

Author contributions

A.A.G., K.E.L., S.D.T., G.B.W., L.M.R., J.T.W., and P.L.H designed the research; K.E.L., S.D.T., G.B.W., A.A.G., Y.E.L., L.M.R., J.T.W., S.J.C., P.A.C., M.T.C.W., and E.N.K. performed the research; K.E.L., S.D.T., G.B.W., A.A.G., Y.E.L., L.M.R., J.T.W., S.J.C., M.T.C.W., E.N.K., J.S.K., and J.D.C.C. analyzed the data; K.E.L., S.D.T., G.B.W., L.M.R., A.A.G., and P.L.H. wrote the paper. All authors provided feedback and approved the final manuscript.

Additional information

Data Deposition: The CS-Rosetta determined ensembles of the N- and C-terminal domains have been deposited in the PDB with accession codes 6CZT and 6D10, respectively. Relevant NMR data has been deposited to the BMRB under accession code 30450.

Competing Interests: The authors declare that they have no conflicts of interest with the contents of this article.

FIGURES

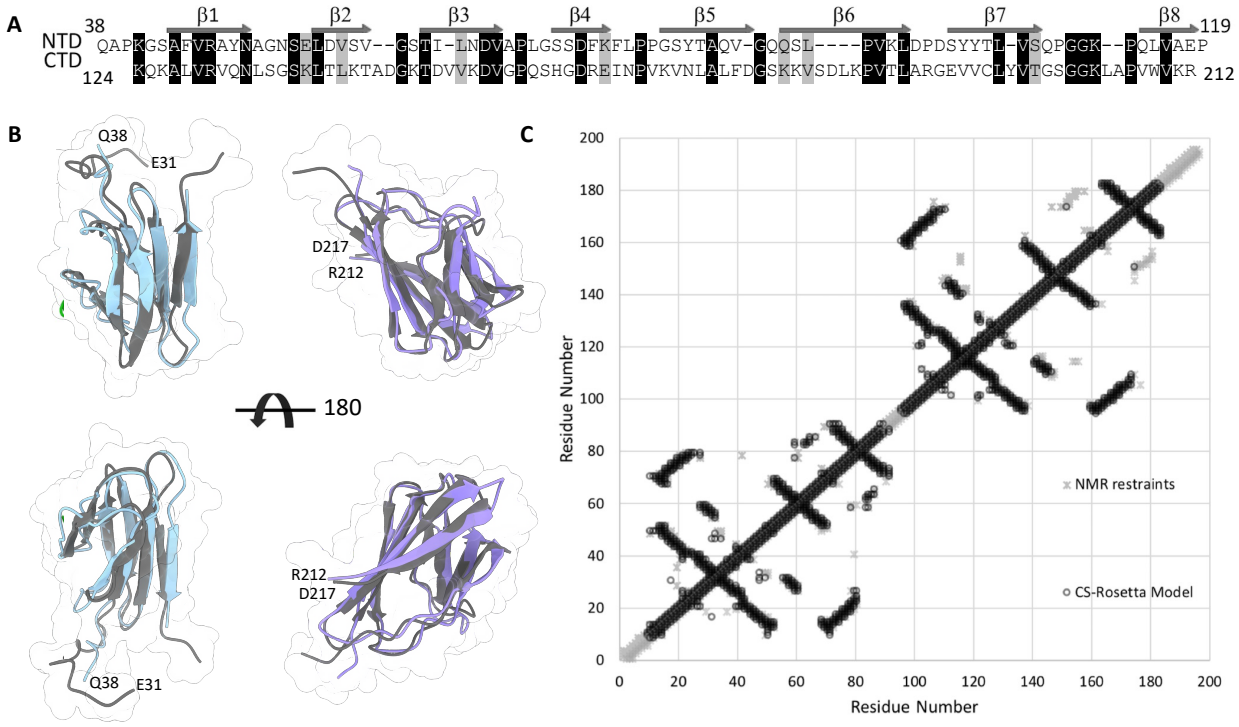

Figure 1: Comparison of CS-Rosetta and NOE derived structures. (A) Sequence alignment of N-terminal (residues 38-119) and C-terminal (residues 124-212) domains of $AlgF_{Pa}^{30-216}$. Identical residues are shaded in black, similar residues are shaded in grey. Secondary structure elements are shown for each domain with secondary structure elements labeled across the top. (B) Superposition of the lowest energy CS-Rosetta (N-terminal blue, C-terminal purple) and NOE-based CYANA structures (lowest energy model in dark grey). The terminal residues are labeled. (C) Contact map analysis between the CS-Rosetta and NMR determined models. The inter-residue contacts observed in the NMR restraint derived model and the CS-Rosetta derived model are shown in grey asterisks and black circles, respectively. The inter-residue contacts are closely mirrored in structures determined by either method showing the similarity shared by the structures determined by independent methods.

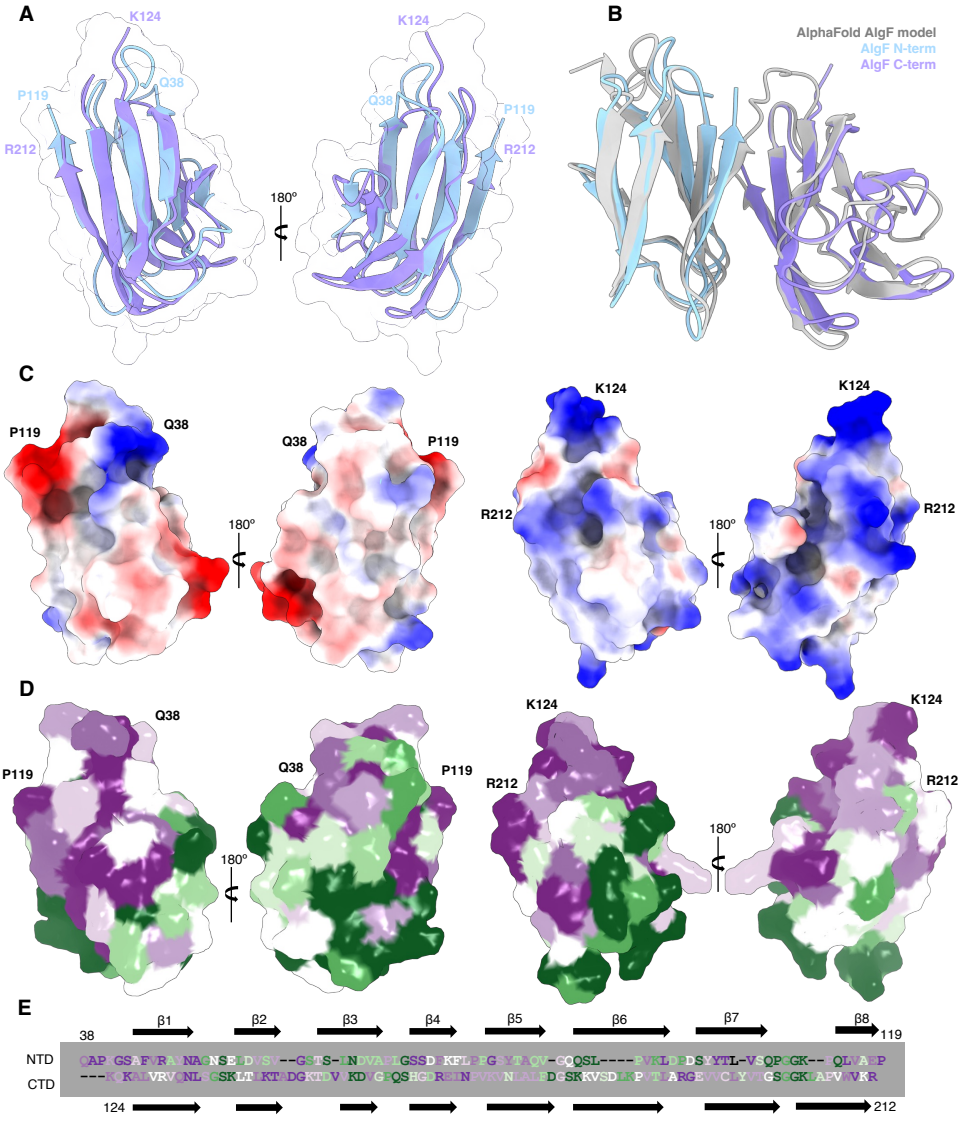

Figure 2: Comparison of the AlgF$_{Pa}$ N- and C-terminal domains. (A) Superposition of N- (model 9) and C-terminal (model 1) domains with an RMSD of 1.35 Å. The average backbone RMSD for the N- and C-terminal domain ensembles is 2.1 Å. (B) Structural superimposition of the N- and C-terminal domains of AlgF$_{Pa}$ with the AlphaFold model of AlgF$_{Pa}$. (C) Electrostatic potential surface representations of the N- and C-terminal domains (left and right, respectively). Shown in same orientation as panel A. The coulombic potential range from -10 (red) to 10 (blue) kcal/(mol · *e*). (D) ConSurf analysis of conserved residues in the N- and C-terminal domains (left and right, respectively). Shown in same orientation as panels A & C. Surface representation colored by level of conservation (green variable to purple highly conserved). (E) Sequence alignment (as in Figure 1) coloured by conservation level.

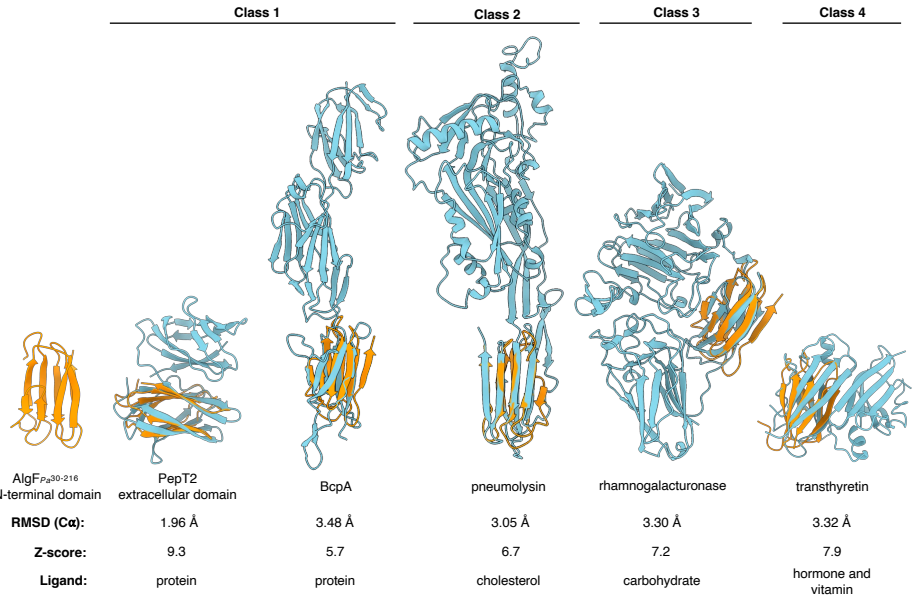

Figure 3: Structural homologs of AlgF bind a variety of ligands. Structural superimposition of AlgF$_{Pa}$ N-terminal domain (orange) with protein structures (teal) representing most (> ~60%) of the overall hits identified using the DALI server to the N-terminal domain of AlgF$_{Pa}$. C$_\alpha$ atom RMSD values and Z-scores for homologous structures are as indicated. The ligand or proposed ligand of the β-sandwich domain for each protein hit is indicated. Classes were defined by the nature of the ligand. The same hits were found using DALI when the C-terminal domain of AlgF$_{Pa}$ and the AlphaFold model of AlgF$_{Pa}$ were used as the search structure. The DALI Z-scores represents a similarity score that considers the distances between C$_\alpha$ atoms between two proteins. (PDB codes left to right: 5A9H, 3KPT, 5AOE, 2XHN, 6R66).

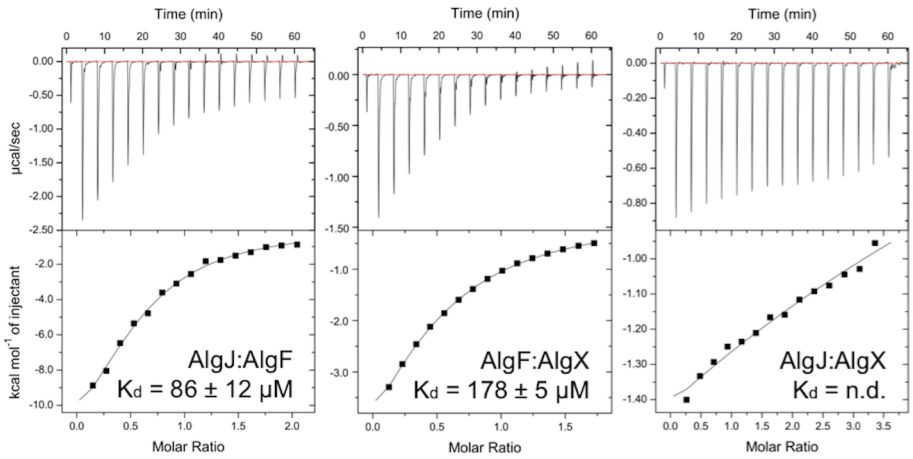

Figure 4: ITC analyses of AlgF$_{Pp}^{29-215}$ protein-protein interactions with AlgJ$_{Pp}^{75-370}$ and AlgX$_{Pp}$. Protein-protein interactions were investigated by binary titrations of AlgJ:AlgF (left), AlgF:AlgX (centre) and AlgJ:AlgX (right) using ITC. Data were fit and analyzed with the Origin software package as shown, and K_d values were determined. The AlgJ:AlgX interaction (right) was too weak to be analyzed.

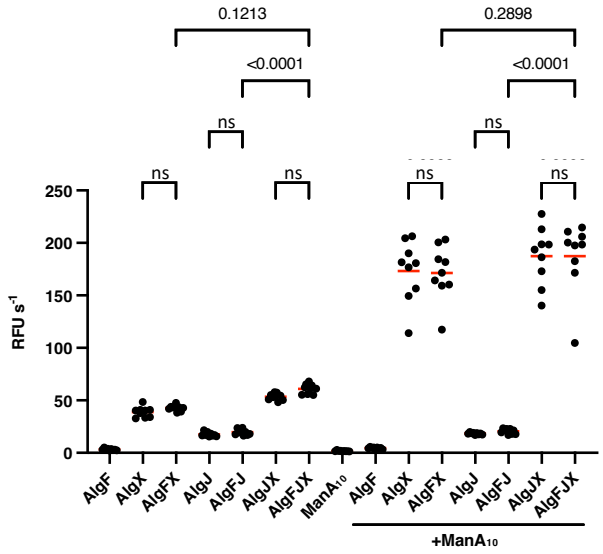

Figure 5: Acetylesterase activity of AlgF and the putative acetylation complex. Enzyme activity was measured by hydrolysis of acetate from the pseudosubstrate ACC. Release of the 7-hydroxycoumarin-3-carboxylic acid fluorescent product was measured (λ_{ex} = 386 nm and λ_{em} = 446 nm). Values represent three technical replicates for three biological replicates. Red lines represent the mean. The reactions were performed with the addition of 2 mM ACC to 5 μM of each protein. Buffer contained 50 mM sodium HEPES pH 7.6 and 75 mM NaCl at 25 °C. $ManA_{10}$ denotes the addition of 1 mg/mL chemically synthesized polymannuronate decasaccharide.

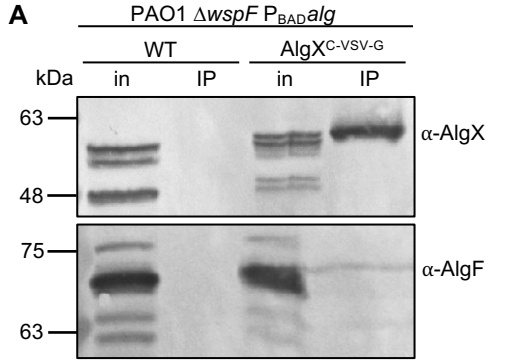

B

Average spectral counts

	Wild-type	AlgX$^{C-VSV-G}$
AlgX	2	185
AlgF	4	161
AlgK	3	242
Alg44	0	1
AlgE	0	1
AlgD	0	4
AlgA	1	1

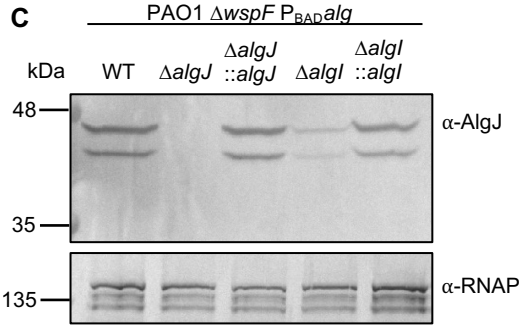

Figure 6: AlgX-AlgF and AlgI-AlgJ interact in *P. aeruginosa*. (A) Co-IP from whole cell lysates of *P. aeruginosa* expressing VSV-G-tagged AlgX as the bait. Proteins applied to the anti-VSV-G co-IP resin (input, in) and the elution from the resin after washing (IP) were analyzed by Western blot using AlgX- and AlgF-specific antibodies. A strain expressing untagged AlgX was used as a negative binding control. (B) Analysis of co-IP eluates from the experiment described in panel *A* by ESI-MS. Spectral counts were the average of six independent co-IP experiments using AlgX$^{C-VSV-G}$ as the bait. Only alginate biosynthetic proteins identified with a minimum of one spectral count in this analysis are listed. (C) Western blot analysis of whole cell lysates of the indicated *P. aeruginosa* strains using AlgJ-specific antibodies. Antisera recognizing the β-subunit of RNA polymerase was used as a loading control.

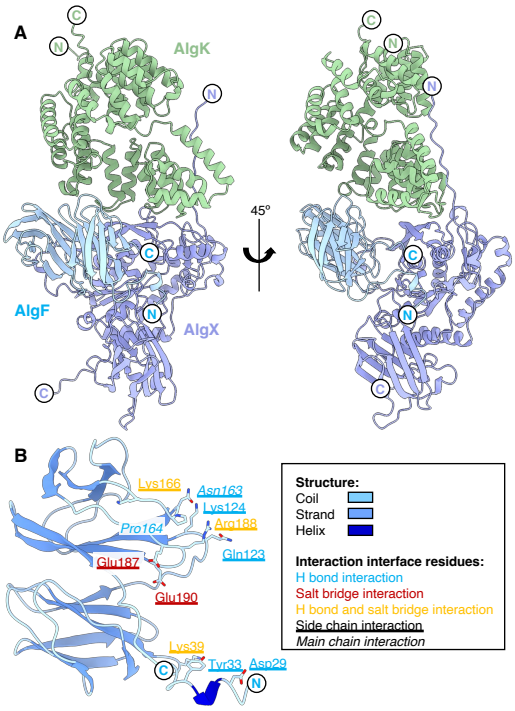

Figure 7: Model of the AlgKXF$_{Pp}$ complex involved in alginate acetylation and export. (A) AlphaFold2 model of the *P. putida* AlgKXF complex (AlgK$_{Pp}$, green; AlgX$_{Pp}$, periwinkle; AlgF$_{Pp}$, light blue). (B) AlgF$_{Pp}$ residues involved in the interaction interface with AlgX$_{Pp}$. The model of AlgF$_{Pp}$ is coloured by secondary structure (coil, light blue; strand; blue; helix, dark blue). Residues involved in hydrogen bonding interactions, salt bridge interactions, or hydrogen bonding and salt bridge interactions are represented by blue, red, and yellow text, respectively. Residues that are underlined represent side chain interactions and residues that are italicized represent main chain interactions. In both panels the N - and C-termini are represented by N and C, respectively.

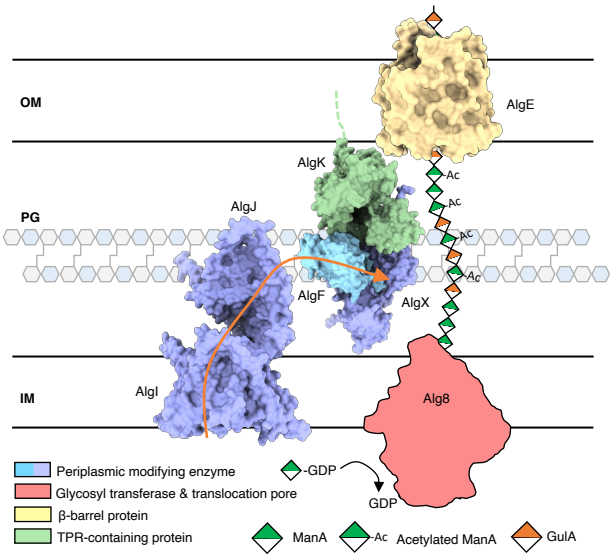

Figure 8: Model of alginate *O*-acetylation machinery. AlgI receives an acetyl group from an as-yet unknown donor in the cytoplasm and the acetate group is passed through the inner membrane and transferred to AlgJ. AlgF mediates interactions in the periplasm allowing for the acetate to be passed from AlgJ to AlgX, where AlgX *O*-acetylates the newly polymerized mannuronic acid. OM, PG, IM denote the outer membrane, peptidoglycan, and inner membrane, respectively. Orange arrow indicates how the acetyl group is transferred between AlgI, AlgJ, and AlgX.

Table 1: Summary of model statistics for AlgF$_{Pa}^{30-216}$

	CS-Rosetta		NOE derived	
	N-terminal domain	C-terminal domain		
Experimental restraints				
CS-Rosetta input			CYANA input	
Residue range submitted	30-119	120-222	Assigned chemical shifts (%)	2043 (94.6)
Folded Core[a]	38-119	124-212	Short range restraints[b]	2267
$^{13}C^{a}$ shifts	88	103	Medium range restraints[b]	438
$^{13}C^{b}$ shifts	79	94	Long range restraints[b]	2145
$^{13}C'$ shifts	84	100	Angle restraints	238
^{15}N shifts	75	95	H-Bond restraints	130
$^{1}H^{N}$ shifts	75	95		
$^{1}H^{a}$ shifts	98	111		
Assigned chemical shifts (%)	914 (93)	1148 (94)		
Ensemble RMSD values				
Residue range	44-119	127-211	42-120[c]	125-211[c]
Backbone atoms Å (# atoms)	1.38 (304)	1.59 (340)	0.32 (316)	0.24 (348)
Heavy atoms Å (# atoms)	6.23 (1116)	8.83 (1300)	10.77 (1136)	11.67 (1340)
Model Quality Measurements				
Ramachandran statistics[d]				
Most favoured regions (%)	98	95		77.6
Additionally allowed regions (%)	2	4		21.9
Generously allowed regions (%)	0	0		0.4
Disallowed regions (%)	0	1		0.2
Other Quality statistics				
Bad contacts/1,000 residues	1	0		33
Violated restraints	N/A	N/A	Distance > 0.5 Å Angle > 10^{o}	91 0

[a] Resides that were determined by CS-Rosetta to be part of the folded core (regions with chemical shift values close to that of a random coil were truncated by the algorithm prior to fragment generation and model generation)
[b] Definitions for restraint ranges: short range $|i-j| < 1$, medium range $1< |i-j| < 5$, long range $|i-j| > 5$.
[c] The domains are aligned separately as the lack of inter domain contacts generates highly heterogeneous models with regard to relative domain positioning.
[d] Results for CS-Rosetta models from the PDB validation report and for the CYANA based models from the CYANA output. The statistics for the CYANA model are for the full-length protein.